

Science

Transient liquid water near an artificial heat source on Mars

Michael H. Hecht and Ashwin R. Vasavada

Jet Propulsion Laboratory, California Institute of Technology, Pasadena, CA, 91109, USA, michael.h.hecht@jpl.nasa.gov

Citation: Mars 2, 83-96, 2006; <http://dx.doi.org/10.1555/mars.2006.0006>

History: Submitted: March 27, 2006; Reviewed: May 8, 2006; Revised: October 26, 2006 Accepted: November 7, 2006; Published: December 14, 2006

Editor: Oded Aharonson, Division of Geological and Planetary Sciences, California Institute of Technology

Reviewers: Hugh Kieffer, Retired, United States Geological Survey; Timothy N. Titus, Astrogeology Research Program, United States Geological Survey

Open Access: Copyright © 2006 Hecht and Vasavada. This is an open-access paper distributed under the terms of a [Creative Commons Attribution License](http://creativecommons.org/licenses/by/3.0/), which permits unrestricted use, distribution, and reproduction in any medium, provided the original work is properly cited.

Abstract

Background: We consider the response of an icy regolith to a localized heat source using analytical and numerical models. Our motivation is to understand the implications of a landing failure in which a radioisotope power source is deposited along with terrestrial microbes within or near icy regolith, resulting in the production of liquid water and the proliferation of microbes.

Method: Our 2-D numerical simulation accounts for temperature-driven phase changes between ice, liquid, and vapor, the diffusion of liquid and vapor through a porous regolith, and evaporation at the surface. Regolith thermophysical properties vary with the abundance of ice and liquid.

Conclusion: We find that liquid water forms and persists for up to 100 sols in cases with the highest initial ice content. However, nearly all the locations that contain liquid are subsequently heated to temperatures that would sterilize any microbes. The exceptions occur for a fully ice-saturated regolith, at depths at least 0.4 m below the surface. Liquid water never appears at the surface itself.

Introduction

Over the next few decades, NASA envisions sending increasingly sophisticated robotic missions to Mars' surface, building toward an eventual human presence. An enabling requirement is abundant and reliable power, leading to the consideration of radioisotope power sources (RPS) such as those used on the Viking landers and other deep space missions. Typical modern RPS are powerful and long-lived, but the conversion from thermal to electrical power is inefficient. For example, an RPS may generate ~2000 W of waste heat while providing ~100 W of electrical power to the spacecraft (although some of the waste heat may be used for the thermal maintenance of the spacecraft) (Abelson et al. 2005).

The delivery of an RPS to Mars' surface raises issues of "planetary protection," that is, ensuring minimal proliferation and dispersal of terrestrial organisms until a definitive search for life on Mars is completed. The present study is concerned with how the heat from an RPS might alter the thermal environment and the state and distribution of water in the

near-surface layer on Mars. A scenario of special concern is a landing failure over ice-rich terrain, in which the RPS (or its fragments) and terrestrial microbes become embedded within the near-surface layer in close proximity to regolith water. Is the heat from an RPS capable of generating transient liquid water, thereby creating a non-equilibrium, habitable environment? Specific conditions needed for survival and propagation of microbes, a complex subject, is outside the scope of this paper. Here we only attempt to establish the amount and persistence of any resulting liquid.

In what follows, we describe a numerical model of the near-surface layer on Mars that considers the transport of heat, liquid, and vapor through a porous regolith. Water can evolve between the solid, liquid, and vapor phases in response to changing temperatures and vapor abundances. In turn, the thermophysical properties of the regolith are modified self-consistently as the water state and distribution change. In these respects, our model follows current simulations of Martian permafrost, most of which use one-dimensional (1-D) formulations for the subsurface (e.g., [Mellon et al. 2004](#); [Schorghofer and Aharonson 2005](#)).

However, some aspects of our study are novel to the existing Mars literature. First, we are interested in the transient response to a high-power heat source. Fluxes of heat and vapor are much larger than those in climate simulations. Second, our priority is to accurately capture the evolution over hours and days, rather than only a final equilibrium state. Finally, our heat source is localized, requiring a 3-D model geometry, calculated in 2-D with the assumption of axial symmetry.

We begin with a brief discussion of liquid water on Mars under present conditions. We then present a one-dimensional steady-state analytic formulation that provides insight into the underlying physical phenomena and helps to validate the results from the more complex numerical model. In the remaining sections, we discuss the geometry, physical parameters, and algorithms of the numerical model, discuss the application of our model to the scenario described above, and present our conclusions.

Liquid Water on Mars Under Present Conditions

Mars has a hydrological cycle similar to Earth's, in the sense that water moves seasonally between reservoirs in a nearly closed cycle (Richardson et al. 2002; Houben et al. 1997; Jakosky 1985). However, on Mars the exchanges occur between the atmosphere and surface condensate, without liquid precipitation or surface flow. The annual temperatures experienced by Mars' primary exposed water reservoir, the north polar ice cap, set the atmospheric vapor concentration. The annually and globally averaged vapor concentration of tens of precipitable microns (pr- μm) corresponds to a frostpoint temperature of $\sim 196\text{K}$, defining the latitudes and depths where ice is stable. At the poles, water ice is stable at the surface. At high latitudes, the zone of ice stability drops centimeters or tens of centimeters below the surface. Ground ice there is insulated from diurnal or seasonal temperature swings and persists in diffusive equilibrium with the overlying atmosphere (e.g. Mellon et al. 2004).

The Gamma Ray Spectrometer (GRS) suite on Mars Odyssey has detected vast hydrogen anomalies (as a proxy for ice) in the locations predicted by equilibrium models, but also found small concentrations in Mars' tropics and equatorial region (Boynton et al. 2002; Feldman et al. 2002; Mitrofanov et al. 2002). In those regions, water is generally unstable as adsorbate or ice, but may exist for long periods of time in disequilibrium or energetically bound to minerals. Potential ground ice at tropical and equatorial latitudes, and morphological features suggestive of recent seepage and flow of liquid water (Malin and Edgett 2000), require more subtle explanations than an equilibrium water cycle.

While on Earth liquid exists over a 100K temperature range at sea level, on Mars the difference between the melting and boiling points is only a few degrees even at the lowest elevations, and at high elevations the atmospheric pressure drops below the triple point entirely. Nonetheless, from a thermodynamic standpoint, the conditions necessary for

liquid, non-boiling water are achieved on Mars presently. Surface temperatures and pressures exceed the triple point values of 273K and 6.1 mbar seasonally over a wide range of latitudes. The absence of liquid in practice is due to the lack of a resupply mechanism such as precipitation. Any liquid in a warm region would evaporate and eventually be trapped in a permanently cold location on a time scale that is rapid compared with slow seasonal and climatic variations in insolation (Ingersoll 1970; Hecht 2002). At 273K on Mars, the evaporation rate is comparable to the rate at 308K (35°C) on Earth (Hecht 2002), about 0.6 mm/hr in the absence of winds. Melting point depression, discussed later, may modestly increase stability, but stagnant water is short-lived at even a small fraction of this evaporation rate. Thus, for liquid water to persist, there must be both sufficient heating and a regular resupply of ice.

As on Earth, ice can be lost to sublimation before ever reaching the liquid state if the frost/dewpoint is below the melting point and heat is applied at an insufficient rate. All stable ground ice on Mars is near or below the average frost point of $\sim 196\text{K}$. Any ice brought toward the melting point by seasonal and climatic forcing will tend to sublimate at a rate far faster than on Earth due to the lower atmospheric pressure. The low frostpoint and high sublimation rate thus conspire to make transitions through the liquid phase unlikely (Ingersoll 1970; Hecht 2002). However, given a heating rate sufficient to warm ice to the melting point and overcome evaporative cooling, ice will transform into a metastable liquid as long as its vapor pressure does not exceed the ambient atmospheric pressure and induce boiling.

In summary, on present-day Mars, liquid water is unlikely except as the result of a quick and dramatic change in environmental conditions such as from a landslide that exposes buried ice to sunlight (Costard et al. 2002), or from the introduction of an artificial heat source, as discussed below. With a frostpoint typically 77K below the melting point, any such water is ephemeral on a geological time scale. The question addressed here is whether it will persist on a biological time scale.

One-Dimensional Steady-State Model

A 1-D analytical formulation of a heat source buried far from the surface in an icy regolith proves to be a useful path to an intuitive understanding of the physical processes and can be used to estimate the extent and persistence of any liquid water generated. It also serves to indicate the relative importance of different parameters and allows interpolation or extrapolation between and beyond the results of more complex and CPU-intensive numerical simulations. In particular, the 1-D equilibrium formulation points to the primary importance of thermal conductivity, as determined by ice content.

The simplest 1-D model assumes a spherically symmetric medium with time-invariant thermophysical properties. At the center of the sphere is a constant-power heat source. When the system has reached equilibrium, the same heat

flux must pass through every radial shell for the system to remain in steady state. The temperature profile is determined by integrating the heat conduction equation in spherical coordinates:

$$\frac{q}{4\pi r^2} = k \frac{dT}{dr} \quad (1)$$

$$q = 4\pi k r (T - T_{ff}) \quad (2)$$

where q is the power output of the heat source, k is the regolith thermal conductivity, T is the temperature at a distance r from the point heat source, and T_{ff} is the far-field temperature (i.e., the radial boundary condition). This profile is illustrated in Figure 1 (top), where R_c , the critical radius, is defined as the radius where $T = 273\text{K}$ in steady state. If k varies with radial distance, the steady state temperature profile can still be determined by integrating this equation *inward* from infinity. As the heat source is approached from a distance, the temperature rise across any shell is inversely proportional to the value of k for that shell.

Of particular interest is the case where an inner sphere, having been purged of ice by the heat source, is surrounded by an infinite icy medium with the boundary at a temperature T_{dry} (typically at or below 273K). In that case,

$$T_2(r) = T_{ff} + \frac{q}{4\pi k_2 r} \quad (3)$$

$$T_1(r) = T_{dry} + \frac{q}{4\pi k_1} \cdot \left(\frac{1}{r} - \frac{1}{R_{dry}} \right) \quad (4)$$

where $T_1(r)$ and k_1 are for the dry inner sphere, $T_2(r)$ and k_2 are for the rest of the medium, and R_{dry} is found from Equation 3. This result, illustrated in Figure 1 (bottom), shows the inflections in the temperature profile resulting from a steep thermal gradient in the insulating dry zone and a shallower gradient in the more conducting icy zone.

If the temperature near the heat source exceeds the boiling point of water, three zones of stability are created. In the far field, water is stable only as ice. In the near field, it is stable only as vapor. A shell between these two zones, bounded by isotherms at the melting and boiling points, defines the region where water is stable as liquid. Before the equilibrium state is reached, this zone moves slowly outward as heat diffuses.

The maximum spatial extent of liquid water is found by solving Equation 2 for the radius where $T = 273\text{K}$. Any liquid water that seeps past this critical radius would quickly freeze. The spatial extent is independent of any change in regolith properties inside the critical radius, including water or ice content. In fact, the only plausible means of altering the stability of liquid outside this radius is if the thermal conductivity there were to decrease, by the further sublimation of ice for example.

The zones described above refer to the stability of liquid water, but stability is a necessary but not sufficient condition for the presence of liquid water. If insufficient heat is provided, all the ice in the regolith at a particular radius may sublimate before the melting point is reached. A more restrictive upper limit to the extent of liquid may be calculated by equating the power going into sublimation (with T just below the melting point) to the output of the heat source. Thus,

$$R_{sh} = \left(\frac{q}{4\pi L_s E} \right)^{1/2} \quad (5)$$

where L_s is the latent heat of sublimation and E is the sublimation rate calculated assuming evaporation by free convection as derived by Ingersoll (1970).

The critical radius, R_c , and the “sublimation horizon”, R_{sh} ,

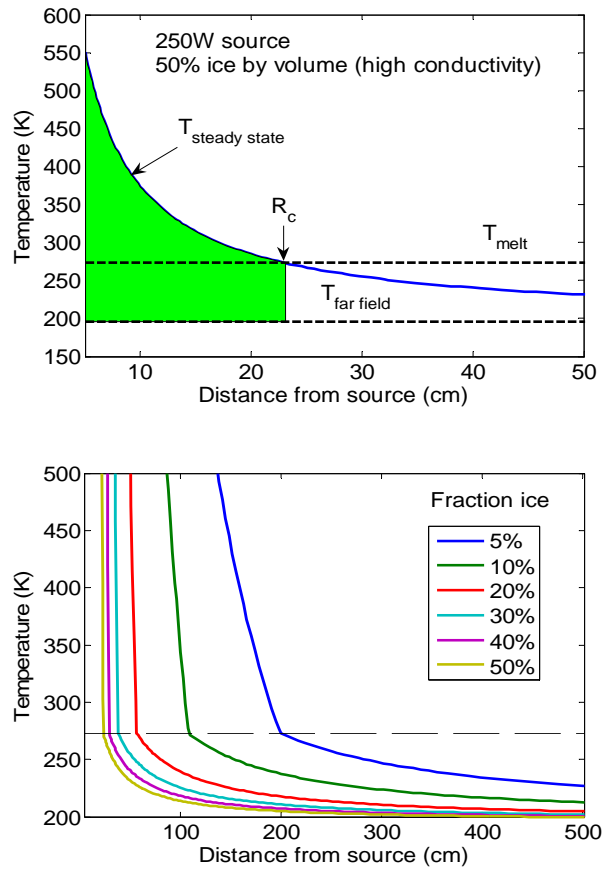


Figure 1. Top: Steady-state temperature distribution around a 250 W heat source in a fully saturated icy regolith (50% ice by volume) initially at 196K. Melting cannot occur where $r > R_c$, corresponding to a temperature contour of 273K. Bottom: Steady-state temperature distribution around a 250 W heat source in a medium that is dry where $T > 273\text{K}$ and contains various volume fractions of ice where $T < 273\text{K}$. The temperature in the far field is 196K.

are two useful metrics to which we will refer in the following sections. Respectively they describe the liquid stability (273K) isotherm at equilibrium and the distance at which latent heat effects make it impossible to warm ice to 273K for a fixed input power. The sublimation rate should not depend strongly on the ice content of the regolith, assuming that it is limited by mixing of the ambient air. Thus, while the critical radius is a strong function of conductivity, and hence ice content, the sublimation horizon is not, as shown in Figure 2 (top). Even in a numerical model that allows temperature and water to evolve over time, the extent of melting is unlikely to exceed the smaller of the sublimation horizon or the critical radius. It may well be less than either of these numbers, since the definition of the sublimation horizon neglects heat loss by simple conduction through the ice.

Several general characteristics can be inferred from Figure 2 (top). For low ice abundances, R_c is greater than R_{sh} , suggesting that the range over which water forms is limited by sublimation. All water that does form is eventually heated to high temperatures ($T \gg 273K$). For higher ice abundances, the equilibrium temperature limits the extent of water formation. In all cases, the temperature gradients are very steep. The spatial separation between volumes in the subsurface at the melting point, boiling point, and microbial sterilization point (assumed to be $\sim 383K$) is quite small. Figure 2 (middle) shows how R_c and R_{sh} vary with input (RPS) power. Both metrics increase with input power, so wet regions will be more extensive for higher input powers. For higher power (depending on initial ice abundance), R_{sh} falls below R_c , ensuring the eventual sterilization of regions where water had the potential to form.

Finally, it is apparent from Figure 1 that the central temperature in the dry limit greatly exceeds the failure point of RPS materials. Pragmatically this would result in melt-down and dispersal of the radioactive material. While we have not modeled this case in detail, qualitatively it expands the spatial extent of the heat source but does not change the net rate of heat generation from that source. Neither the limit of modest dispersal in the quickly-drying central zone nor violent dispersal into small, localized sources would result in a greater microbial hazard than a concentrated heat source.

Two-Dimensional Dynamic Simulation

In the following sections we describe the details of our 2-D model in general terms, with the belief that it may be applicable to scientific problems beyond our specific, spacecraft-related study. Our immediate goal is to model the response of a frigid, stratified regolith (i.e., dry and icy layers) to the presence of a localized, buried heat source. Here we include several more physical processes than in the 1-D analytical model. Some are only crudely represented due to approximations or uncertainty. However, the formulations described below are expected to allow us to judge the relative importance of different processes in determining the distribution of temperature and liquid water.

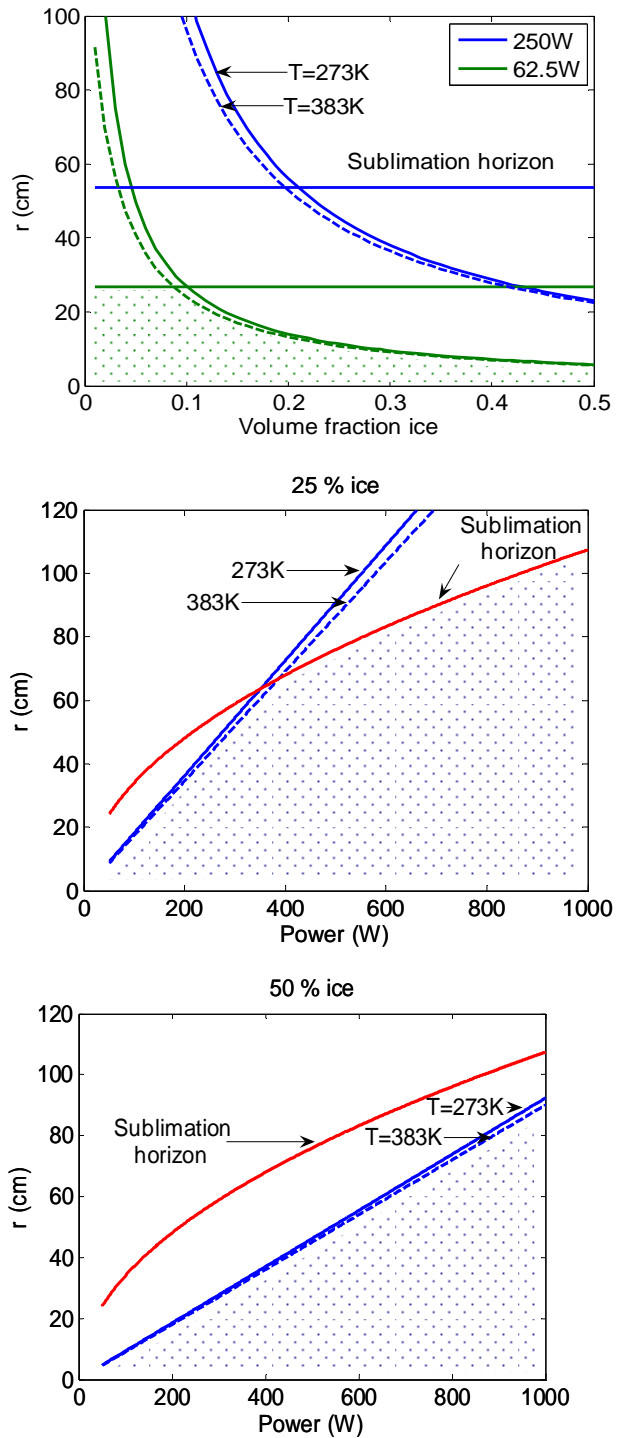


Figure 2: Top: Critical radii (curves) and sublimation horizons (horizontal lines) for 250 W and 62.5 W heat sources in icy regolith initially at 196K. The farthest distance where melting can occur is the smaller of the critical radius and the sublimation horizon (shaded for 62.5 W). Middle: Critical radii (blue lines) and sublimation horizons (red curves) as functions of RPS power, for ice volume fractions of 0.25. Bottom: Same for ice volume fraction of 0.5. Liquid can potentially form in the shaded region, but sterilization occurs below the 383K contour.

Model Domain and Architecture

The scenario described above can be represented by a cylindrical coordinate system with the surface at the top and the heat source located on the axis of symmetry. An example model geometry is shown in Figure 3. The domain of interest extends in the horizontal and downward directions to the distance at which the influence of the heat source becomes negligible. We subdivide the domain using constant increments of radial distance and depth. A volume element, therefore, is a ring with a square cross-section. The increment size is a constant determined by the regolith thermophysical properties. Because the radial increment size is constant, element volumes increase with radial distance.

We use an explicit finite different method on the cylindrical grid, calculating a number of physical processes in sequence at each time step: heat flow, liquid flow, liquid/solid phase change, surface energy balance, and vapor diffusion. The details of each are discussed below. This method is prone to instability unless small time steps are used. The stability scales with the grid spacing in each dimension, and inversely with the diffusion constant and the time per step. While the instability can be reduced by use of an implicit scheme, such methods are not easily implemented when the diffusion constant varies spatially in an indeterminate way. Accordingly, we use as coarse a grid as practical and small time steps.

Regolith Thermophysical Properties

We model the subsurface as a particulate regolith with the same dry thermophysical properties and porosity at all depths. Within the icy layer, ice is present within the pore spaces. The initial interface between the dry and icy layers is sharp.

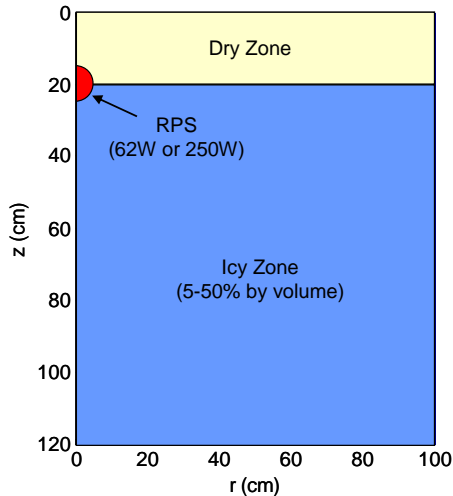


Figure 3: A 0.05 m radius Radioactive Power Source (RPS) is assumed to be buried under a 0.2 m layer of dry regolith and above a zone of mixed ice and regolith. The map is in cylindrical coordinates and represents a vertical (and radial) slice through the three-dimensional domain of our numerical simulation.

The thermophysical parameters of relevance to this model are the bulk density, heat capacity, and thermal conductivity of each element. Each depends upon the fractional volume occupied by regolith, air, ice, liquid, and vapor. The bulk volumetric heat capacity is the sum over the components,

$$\rho c_p = \rho_r c_{p,r} + \rho_{ice} c_{p,ice} f_{ice} + \rho_w c_{p,w} f_w \quad (6)$$

where ρ is density, c_p is the specific heat capacity, and the subscripts r , ice , and w refer to regolith, ice, and water. The variables f_{ice} and f_w are the volume fractions of ice and water. Note that ρ_r already accounts for the fractional volume of regolith (i.e., it is the bulk density of dry regolith). The bulk thermal conductivity is calculated in a similar fashion,

$$k = k_r + k_{ice} f_{ice} + k_w f_w \quad (7)$$

where k_r is the bulk conductivity of the regolith. In a dry particulate regolith, heat transfer is limited by the contacts between grains. Condensation will occur preferentially at these contacts, providing enhanced conductivity even for small volume percentages of water or ice (e.g., [Mellon et al. 1997](#)). Our simple parameterization of conductivity is likely to be an underestimate, but is not expected to change our conclusions significantly. The contributions to the heat capacity and thermal conductivity from air and water vapor are negligible. Latent heats are not included in the thermal conductivities but are calculated explicitly. Thermophysical properties are immediately updated whenever changes occur in temperature or the abundance or phase of water.

The thermophysical properties of dry Martian regolith are derived from orbital surface temperature observations. We have assumed values typical of high-albedo, low thermal inertia materials that are inferred to be deposits of unconsolidated fines ([Putzig et al. 2005](#)). Thermal inertia (driven mostly by the solid and gas thermal conductivities) is expected to be higher for a regolith composed of consolidated fines or larger particles. It is not known how thermal conductivity varies below the centimeter-scale depths relevant to the orbital measurements.

Thermal Diffusion

Heat transport is modeled by numerically integrating the thermal diffusion equation in cylindrical coordinates,

$$\rho c_p \frac{dT}{dt} = \frac{1}{r} \frac{\partial}{\partial r} \left(r k \frac{\partial T}{\partial r} \right) + \frac{\partial}{\partial z} \left(k \frac{\partial T}{\partial z} \right) + \frac{dq}{dt} \quad (8)$$

where T is temperature in degrees Kelvin and t is time in seconds. The last term is calculated by assuming that all of the power from the heat source goes into increasing the internal energies of the volume elements containing it (the term is zero elsewhere).

The values of r and z correspond to the centers of volume elements. The equation is integrated first in the radial

Table 1. Model Physical Parameters.

Parameter	Symbol	Value
Radial Increment (m)		0.05
Number of Radial Bins		20
Vertical Increment (m)		0.05
Number of Vertical Bins		24
Model Time Step (s)		1.44
Density, Regolith (kg m ⁻³)	ρ_r	1400
Density, Ice (kg m ⁻³)	ρ_{ice}	920
Density, Water (kg m ⁻³)	ρ_w	1000
Heat Capacity, Regolith (J kg ⁻¹ K ⁻¹)	$C_{p,r}$	800
Heat Capacity, Ice (J kg ⁻¹ K ⁻¹)	$C_{p,ice}$	2100
Heat Capacity, Water (J kg ⁻¹ K ⁻¹)	$C_{p,w}$	4182
Therm. Cond., Regolith (W m ⁻¹ K ⁻¹)	k_r	0.02
Therm. Cond., Ice (W m ⁻¹ K ⁻¹)	k_{ice}	0.4685 + 48.819/T
Therm. Cond., Water (W m ⁻¹ K ⁻¹)	k_w	0.56
Regolith Porosity		0.5
Regolith Tortuosity	τ	3
Vapor Diffusion Const, STP (m ² s ⁻¹)	D_v	1.63×10^{-5}
Liquid Diffusion Constant (m ² s ⁻¹)	D_h	1.16×10^{-7}
Regolith Infrared Emissivity		0.95
Atm. Surface Pressure (mb)	P_{Mars}	10
Atm. Heat Trans. Coef. (W m ⁻² K ⁻¹)		0.5
Latent Heat of Melting (J kg ⁻¹)		3.34×10^5
Latent Heat of Vaporization (J kg ⁻¹)		2.50×10^6
Latent Heat of Sublimation (J kg ⁻¹)	L_s	2.83×10^6
Kinematic Viscosity of CO ₂ (m ² /s)	ν	6.93×10^{-4}

dimension and subsequently over depth. Each first difference in temperature is multiplied by the average values of k and r between adjacent cells. A far-field boundary condition is applied to the outer and lower boundaries by assuming the second derivative to be equal in the final two rows or columns. Since the surface energy balance is calculated explicitly in a later step, the surface boundary condition assumes $\partial T / \partial z = 0$ across the surface. At the axis, $\partial T / \partial z = 0$ also applies. Sensible heat transferred by the movement of liquid can be ignored due to the small difference between the melting and boiling points and the much larger budgets of latent heat.

Liquid Water Flow

Darcy's Law describes the flow of liquid driven by a gradient in hydraulic potential, ψ , within a soil. The potential can include matric (capillary and adsorptive), gravitational, osmotic, and thermal components. In one dimension,

$$q_w = -K \frac{\partial \psi}{\partial x} \quad (9)$$

where q_w is the flux of water, ψ is the hydraulic potential, and K is the hydraulic conductivity. The practical application of (9) is made difficult by interdependencies between K , ψ , and the soil wetness, θ , and the wide variation of these parameters in natural soils (Hillel 1998). For our purposes, the soil wetness is equal to the volumetric water content, f_w .

As described below, we have parameterized liquid flow using an empirical formulation derived from terrestrial soils, admittedly a vast simplification. No comprehensive theory exists that describes flow for the range of soil properties found on Earth, much less the unknown properties of the Martian regolith. In addition, we have ignored flow driven by gravitational, osmotic, or thermal forces. We use this approximation primarily to assess the relative importance of the process. Flow is only a modest effect--it helps remove water only when very wet. By choosing conservative parameters, we intentionally underestimate one effect that would reduce the persistence of liquid water by removing it from the narrow zone of stability and hence reduce the ability of microbes to propagate.

The mathematical description of unsaturated flow can be simplified by relating flux directly to the gradient of wetness. Flow is cast as a diffusive process analogous to the diffusion of heat,

$$\frac{\partial \theta}{\partial t} = -\nabla \cdot q_w = \frac{\partial}{\partial x} \left[D_h(\theta) \frac{\partial \theta}{\partial x} \right] \quad (10)$$

where D_h is the hydraulic diffusivity, defined as

$$D_h(\theta) = K(\theta) \frac{d\psi}{d\theta} \quad (11)$$

A solution requires knowledge of how both the hydraulic conductivity and potential vary with wetness. However, terrestrial experience suggests that the diffusivity driven by matric potential varies exponentially with wetness, $D_h(\theta) = ae^{b\theta}$, where a and b are empirically determined constants. Following Hillel (1998), we assume that over the full range of wetness (i.e., dry to saturated), D_h lies between factors of 10^{-2} and 10^2 of the typical terrestrial diffusion rate listed in Table 1. This assumption is used to derive a and b , replacing θ with f_w . Finally, D_h is scaled by the fraction of pore space not filled by ice and diffusion is calculated using the same numerical methods (in cylindrical coordinates) as for heat. In performing the second derivative, the value of D_h is chosen corresponding to the direction of the flow so that a saturated cell ($D_h = 0$) will not receive additional liquid.

Solid-Liquid Phase Changes

Phase changes between ice and liquid water are assumed to occur instantaneously as heat is transferred between elements. Excess internal energy relative to the melting point, $\rho_c p(T - 273K)$, melts any ice that is present until either the ice or excess energy is depleted. Likewise, energy deficits drive freezing. Any remaining energy or energy deficit changes the element's temperature. Throughout the simulation, water is treated as chemically pure. Adsorbed and mineralogically bound water is ignored.

Surface Energy Balance

The surface energy balance includes the effects of radiation, sensible heat exchange between the surface and atmosphere via convection, and evaporation. We neglect the diurnal and seasonal cycles of insolation because we are interested only in the response of the regolith to the presence of a strong heat source. Instead, we artificially set insolation (including albedo effects) at a constant value that would maintain the surface at the far-field temperature, T_{ff} , if the heat source were absent.

Processes acting on surface-bounded elements are calculated in the following order. The maximum potential rate of mass loss to the atmosphere is taken to be the equilibrium evaporation rate assuming free convection (Ingersoll 1970). Vapor is allowed to escape first. The rest of the budget is allocated to evaporation of liquid, then sublimation of ice. Latent heat requirements are summed and element temperatures are adjusted accordingly. We next calculate radiation and convective heat transfer and adjust temperatures. If any surface element temperatures remain above the boiling point and contain liquid, the excess energy is used to convert the liquid to vapor.

Ingersoll (1970) and Hecht (2002) propose the following formula for the evaporation or sublimation mass flux ($\text{kg m}^{-2} \text{s}^{-1}$) under free convection:

$$E = (0.17)D_v \Delta C \left[\frac{g}{\nu^2} \cdot \frac{\Delta \rho}{\rho} \right]^{1/3} \quad (12)$$

where D_v is the vapor diffusion constant for H_2O in CO_2 , ΔC is the difference in vapor concentration (mass/volume solute) between the evaporating surface and the surrounding atmosphere (approximately equal to the saturation density of water vapor at the temperature of the evaporating liquid or ice), g is gravitational acceleration, and ν is the kinematic viscosity of CO_2 . The quantity $(\Delta \rho / \rho)$ is the difference between the density of the ambient air and that of the gas at the surface, divided by that of the gas at the surface,

$$\frac{\Delta \rho}{\rho} = \frac{(\rho_\infty - \rho)}{\rho} = \frac{(m_e - m_w)e}{m_e P_0 - (m_e - m_w)e} \quad (13)$$

where ρ is the total density at the evaporating surface, ρ_∞ is the density of the surrounding atmosphere, e is the saturation vapor pressure of the evaporating water (or ice), P_0 is the total atmospheric pressure, m_w is the molecular weight of water, and m_e is the molecular weight of ambient air.

Water Vapor Equilibration and Diffusion

Our modeling of water vapor makes two assumptions. First, the time scale of equilibration is much shorter than the time scale of diffusion (the vapor concentration comes to equilibrium at each time step). Also, ambient gas is able to adjust instantaneously to changes in the partial pressure of water. We do not account for small changes in the enthalpy of vapor and the corresponding sensible heat

exchange via vapor transport. All water is assumed to be in a pure solid, liquid, or vapor phase. Adsorption and other forms of bound water have not been considered, both for reasons of simplicity and because it is not particularly relevant to habitability. Bioavailability of water in soil is measured by water activity, which is equivalent to relative humidity in equilibrium. In other words, water that is chemically bound may not sublime readily, but neither will it support microbial life.

Equilibration is accomplished by exchanging latent heat of vaporization for sensible heat until the temperature and vapor pressure are in balance (i.e. water vapor is just at saturation). The calculation starts by finding the energy density within every volume element due to internal energy ($\rho c_p T$) and latent heat of vaporization (the volumetric abundance of vapor, f_v , multiplied by the latent heat of sublimation for elements where $T < 273\text{K}$, and f_v multiplied by the latent heat of boiling where $T > 273\text{K}$). The equilibrium vapor densities corresponding to these energy densities are taken from a lookup table. Available liquid, and then ice, change phase in order to bring the vapor density toward the equilibrium value. Temperatures are adjusted to provide the required latent heats.

The diffusion of water vapor is calculated using the same numerical methods as for heat and liquid,

$$\frac{d\rho}{dt} = \frac{1}{r} \frac{\partial}{\partial r} \left(r D_v \frac{\partial \rho}{\partial r} \right) + \frac{\partial}{\partial z} \left(D_v \frac{\partial \rho}{\partial z} \right) \quad (14)$$

where the diffusion constant for water vapor is:

$$D_v = \frac{D_{v0}}{\tau} \cdot \frac{P_{STP}}{P_{Mars}} \cdot \left(\frac{T}{T_{STP}} \right)^2 \quad (15)$$

D_{v0} is the diffusion constant for water vapor in CO_2 at standard temperature and pressure, τ is the regolith tortuosity, and the second factor is the ratio of standard pressure to the surface pressure at Mars' surface. The last factor, the ratio of the temperature to 298K squared, is applied after capping the value of T at T_{boil} . Finally, D_v is scaled by the fraction of pore space not filled by ice or liquid.

Results and Discussion

Motivated by a requirement to determine the implications of a landing failure over ice-rich terrain that results in the burial of an RPS surrounded by a halo of microbial contamination, we consider whether the RPS might create environmental conditions (temperature and liquid water) that allow microbes brought from Earth to multiply. Of ultimate importance is the time history at every radius and depth in the vicinity of the RPS, including not only the extent and persistence of liquid water, but also the thermal evolution of the location after it has dried. Temperatures above approximately 383K (110°C) will reduce by many orders of magnitude the population of even the hardiest of

terrestrial microbes that may have propagated when the location was still wet. Thus the scenario that poses the greatest challenge to international Planetary Protection agreements is one in which a volume of icy regolith containing terrestrial microbes is warmed sufficiently to create water that persists for many sols, but never gets sufficiently hot afterward to kill any microbes that may have propagated.

The specifics of the RPS and its assumed burial depth are based upon modern RPS designs (Abelson et al. 2005) and simulations of the atmospheric entry, breakup, and impact of a specific spacecraft design, the details of which are not presented here. The configuration of the surface and RPS shown in Figure 3 was found to represent a plausible but worst-case scenario (i.e., maximum depth penetration with intact RPS elements). Guided by recent results from the GRS suite on the Mars Odyssey spacecraft, we assume the impact site is characterized by ice-rich regolith 0.2 m below the surface. The heat source comes to rest at the interface between dry regolith above and ice-rich regolith below. The complete 2000 W RPS, consisting of eight 250 W modules, breaks up in the impact scenarios considered. The implanted heat source would likely be in the form of a 250 W module or a constituent 62.5 W pellet.

A list of assumed regolith properties and other constants is given in Table 1. At all levels the regolith has a dry density, heat capacity, and thermal conductivity typical of high-albedo, low-thermal inertia regions on Mars. The porosity and tortuosity are poorly known, but we use best-estimate values that are common in the literature. The system is initialized in an equilibrium state (roughly) by setting the atmosphere, surface, and regolith at 196K, corresponding to the annual average frost point.

Two-dimensional simulations were performed for a 62.5 W and 250 W RPS, as well as smaller sources for select cases. The 62.5 W source created liquid only in the case of an initially saturated icy layer. Here we will present results for the 250 W source, which provided a worst-case analysis for all initial ice concentrations. Analyses were performed for different values of ice content in the icy layer, varying from 5% to 50% by volume. As a proxy for thermal conductivity, ice content has the single greatest effect on the spatial extent and persistence of water. At designated intervals of elapsed time (typically every 30 minutes) the simulation outputs maps of key parameters. These maps can be used to create time-lapse movies of the evolution of the three-phase system. The following paragraphs describe snapshots of those data sets.

Figure 4 shows a time series of maps of the temperature, ice content, and liquid water content for an initial (icy-layer) ice content of 40%. The horizontal axis represents radial (horizontal) distance from the center of the RPS out to 1 m, while the vertical axis extends from the surface to a depth of 1.2 m. The horizontal white line indicates the initial boundary between the dry and icy layers, while the hemisphere represents the location of the RPS (modeled

as filling an integral number of model volume elements). The fineness of the grid in each dimension (0.05 m in this case) is roughly proportional to the amount of time required for the simulation, typically several CPU hours per run on a PC. In 3-D space, each cell is a cylindrical ring, and thus the volume of water represented by any cell increases to the right. The total volume of damp regolith (>1% water) never exceeds 25 liters in any simulation.

After emplacement of the RPS, the thermal wave progresses outward with time, eroding the ice roughly symmetrically around the RPS. A thin layer of liquid lines the boundary between the inner dry zone and the outer icy regolith. Water vapor diffusing outward re-condenses in the upper dry zone both as liquid and ice, but in all cases the simulation shows a direct diffusion path between the shell surrounding the RPS and the surface (i.e. the regolith does not become choked off by ice).

Figure 5 maps the peak liquid volume fraction present in every cell at any time in the simulation. Cells closest to the RPS achieve this degree of wetness only ephemerally and early in the simulation, while in the farthest cells the liquid forms later and may persist for many sols. In general the maximum liquid content increases with initial ice content, but in many cases the liquid content exceeds the initial ice content as liquid or vapor diffuses away from the RPS and becomes trapped at the ice boundary. While small amounts of liquid are eventually found in the initially dry (upper) layer, surface transpiration is sufficient to keep the very surface completely dry in all simulations. As a result, we can conclude that microbes are unlikely either to propagate or be carried to the surface where they might be scattered by Martian winds (unless the winds excavate a significant amount of regolith).

Figure 6 shows the temperature distribution 100 sols after the last appearance of liquid anywhere in the simulation. The color scale has been chosen to emphasize the region above 383K, the lower-limit value for dry heat sterilization. As expected, the hot zone surrounding the RPS is highly localized in the case of ice-rich, thermally conducting regolith, while it is significantly more extensive in dry, insulating regolith that cannot efficiently remove heat. Since the extent of the wet zone in Figure 5 is only weakly dependent on ice content, it can be concluded that the any microbes that may have propagated in regolith with *low* initial ice content will be subsequently sterilized.

Figure 7 captures a measure of when the water content of the soil becomes so low that it is unavailable for plants or microbes, or indeed for sublimation and diffusion. In physical terms, the remaining water is held tightly in capillaries, and the relative humidity (or, equivalently, the water activity) drops precipitously while the water retention curve becomes extremely steep. One suggested definition for this hygroscopic limit was the point on the water retention curve corresponding to 15 bar suction (Gardner 1968). As soil retention curves vary strongly

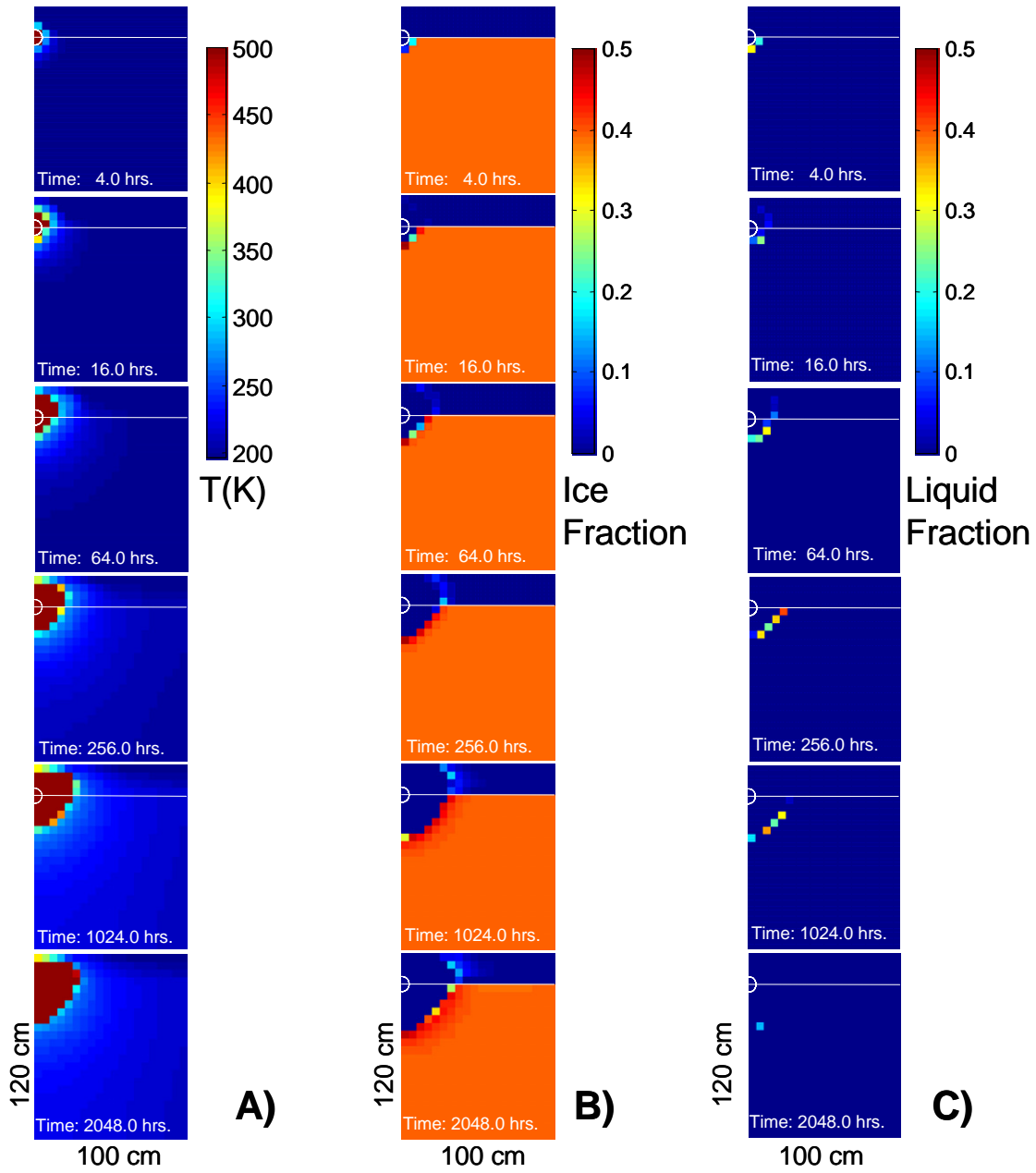


Figure 4. (a) Maps of temperature at various times (4, 10, 64, 256, 1024, and 2048 hrs) for a regolith with an initial ice content of 40% and a 250 W heat source. The color scale is chosen to highlight the sterilization regime above 383K. (b) Same as (a) but showing the time evolution of the ice volume fraction. (c) Same as (a), but showing the time evolution of the water volume fraction.

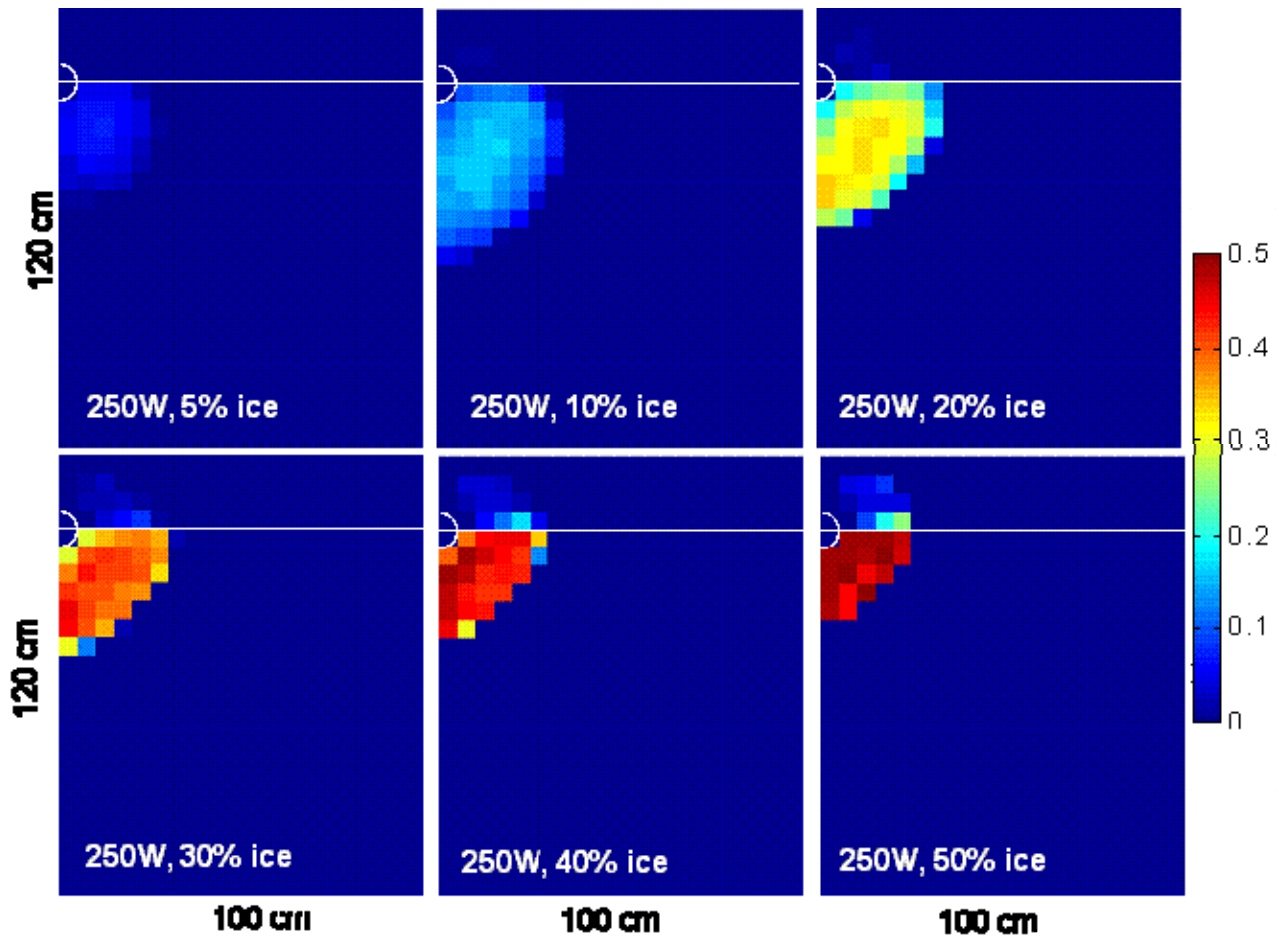


Figure 5. Maps of the maximum liquid content of every cell attained at any time during the simulation. As initial ice abundance increases from 5% to 50%, the range of liquid decreases but its abundance increases. Note that the maps do *not* represent a snapshot in time, but are akin to time exposures as the thermal wave travels out from the RPS.

with soil type, we have selected 4% by mass as a conservative (low) value for loam-type soils. Figure 7 (top) displays the total time that each cell contained more than 4% liquid by mass in the simulation.

Figure 7 (bottom) shows the same data, displaying only the cells where the temperature has not yet exceeded 383K by the elapsed time indicated. Sterilization occurs quickly and completely for initial ice contents of 5%, 10%, and 20%, which are not shown. For cases with higher initial ice contents, two snapshots in time are displayed. In all cases except the fully saturated (50%) case, all cells that ever contained liquid water are completely sterilized within 400 sols after the last appearance of liquid. In the 50% case, the outermost wet cells remain at sub-sterilization temperatures for over 1100 sols (the longest simulation performed). The system has approached thermal equilibrium by this time, but temperatures continue to evolve as ice sublimates at the margin of the dry zone. While a strong function of temperature, the rate of sublimation of ice does not have a distinct inflection at 273K, and the latent heat of sublimation is equivalent to the combined latent heats of melting and evaporating.

Thus ice will continue to retreat past R_{sh} or R_c at temperatures less than 273K, at an ever-decreasing rate. For the ice-rich cases, the steep thermal gradient inside the dry boundary results in a significant change in the temperature of the once-wet cells.

While the dynamic simulation provides more accurate and detailed results, there are many possible independent variables, and to run each case individually is time-consuming. Accordingly, it is useful to evaluate the steady-state model to establish trends as a function of parameters such as volume fraction of ice. Figures 8 and 9 compare the 1-D analytical steady-state model with the 2-D numerical simulation. Figure 8 compares calculations of R_c and R_{sh} with the locations of the most distant cells containing liquid water in the 2-D simulation. Note that these radii are an upper limit on where water may form, so the expectation that simulated values will fall below the calculated limits is satisfied. The spatial resolution of the simulation is approximately the diagonal distance across the 0.05 m cell in the 250 W RPS case (or 0.025 m for the 62.5 W RPS). It appears that water approaches the limiting radius to within this resolution. A possible exception is a drop off in spatial extent for the driest soils.

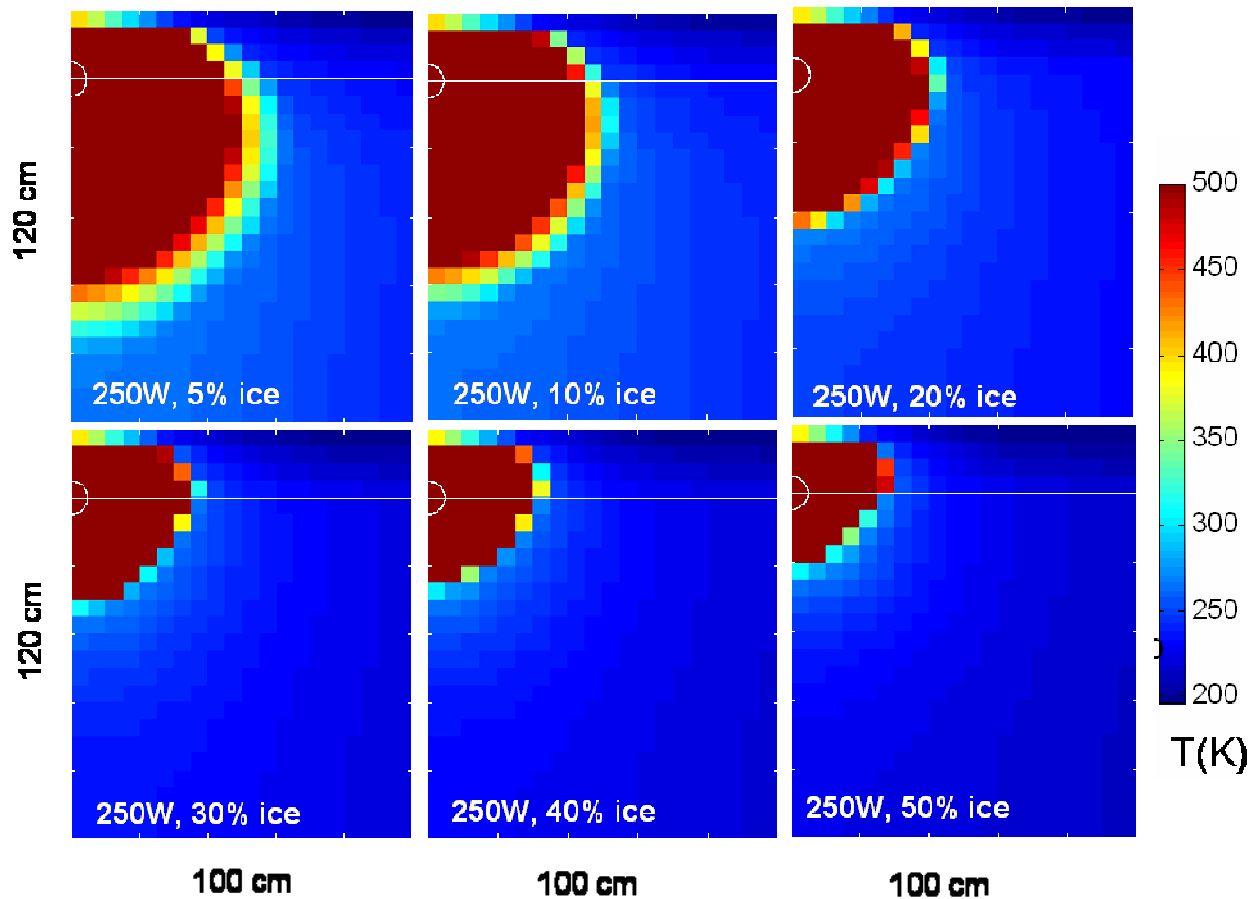


Figure 6. Maps of temperature reached 100 sols after the disappearance of liquid from the simulation. The scale has been chosen to emphasize regions that are sterilized by exposure to temperatures above $\sim 383\text{K}$.

This behavior is not surprising since a much larger fraction of the heat escapes to the far field when the difference in thermal conductivities between the dry and icy zones is small. Of particular importance is the range of initial ice contents where R_c exceeds R_{sh} . In these cases, ice is expected to continue to retreat to R_c by sublimation, even though no liquid forms past R_{sh} , and the once wet cells eventually become extremely hot.

Figure 9 compares the simulated persistence of water (crosses) to the time required to completely sublimate all the ice up to the smaller of R_{sh} and R_c . For the 1-D calculations we assume that 50% of the RPS heat is absorbed within a sphere bounded by the smaller of R_c and R_{sh} , and that 25% of that heat goes into warming or sublimating ice (the remainder goes into warming dry regolith). The first assumption allows liquid to persist longer since less heat is available for sublimation. The second assumption reduces the persistence by reducing R_{sh} . Again the biggest deviation is for low initial ice content, where the first assumption is an underestimate. These assumptions are intuitively plausible when compared to snapshots of the thermal gradient after the last water has disappeared.

We have also considered several special cases that may

significantly alter the above results. For example, any scenario that seals the wet zone from the surface would allow liquid to persist indefinitely. This can not be accomplished with ice alone, since in all plausible cases, the ice above the RPS will be warmer than the surrounding surface and will eventually sublimate. Hypothetically, the surface may be sealed by a physical obstruction such as a large boulder or spacecraft debris. Our simulations show that such obstructions would have to extend to the radial distance over which vapor escapes (similar to R_c or R_{sh}) in order to influence the results, an unlikely scenario because the RPS is not expected to come to rest below large natural obstacles and because the only sufficiently large spacecraft pieces (e.g., the back shell) are unlikely to land near the RPS.

If the RPS were deposited in a sheet of solid ice and the constraints of the model are relaxed to allow the RPS to move, it is found that it would descend through the ice at a rate of several centimeters per hour, surrounded by a bubble of liquid. Any microbes allowed to propagate in this environment would end up buried well below the surface.

We also considered how higher far-field temperatures might influence our results. Our 1-D arguments suggest that unsterilized wet regions would be less likely to occur relative to our nominal cases. Although R_c would be larger, R_{sh}

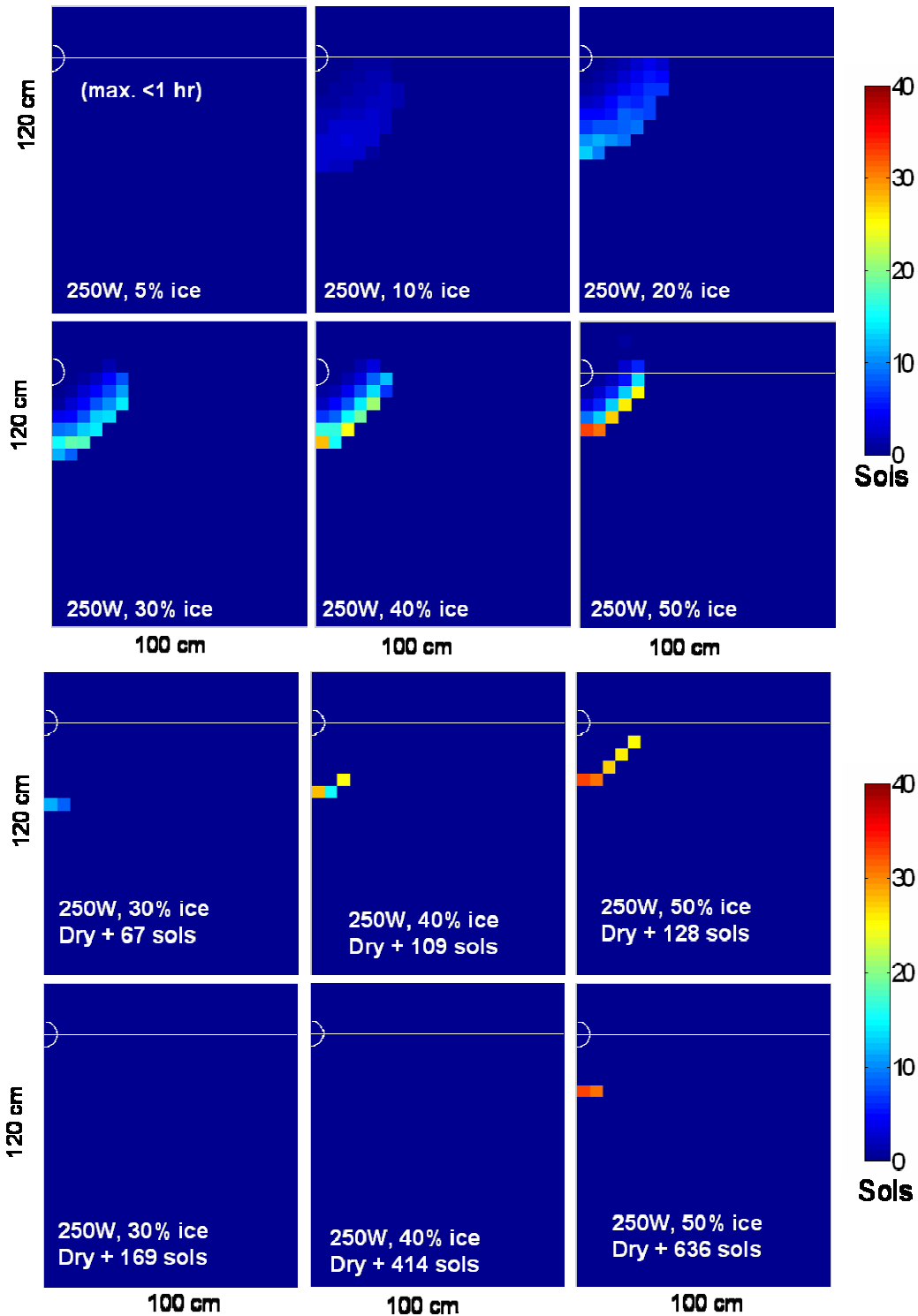


Figure 7. Top: Maps of the persistence of liquid water. Cells are color-coded to show the total time that each cell contained more than 4% water *by mass*, a nominal minimum value for the propagation of microbes. Cells near the dry layer boundary (0.2 m line) are most likely to contain microbes initially. Liquid persists the longest in the case with an initial ice volume fraction of 50%, offering a habitat for up to 15 sols near the dry layer and 35 sols at greater depth. Bottom: Maps of the persistence of liquid and the occurrence of heat sterilization. The colored cells both contain more than 4% water by mass at some time during the simulation and have temperatures not exceeding 383K at the indicated time after drying. The scale indicates how long the cell was wet. No cells meet the criteria for < 30% ice. The 30% case reaches sterilization temperatures by 160 sols, the 40% case by 400 sols. Even after a Martian year, the two deepest “wet” cells remain unsterilized in the 50% case (this was still true nearly an additional year later).

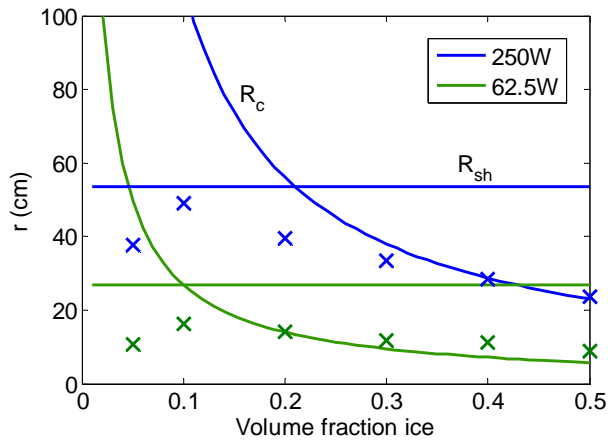


Figure 8. Comparison of calculated critical radii (curves) and sublimation horizons (horizontal lines) with numerical results (crosses). Crosses indicate the greatest radius at which liquid water is found in the 2-D simulation (above 0.1%). Results for both 250 W and 62.5 W sources indicate that the range is not strongly sensitive to the ice content. Note that the cells are 0.05 m squares for the 250 W case and 0.025 m squares for the 62.5 W case.

would remain the same. The hot zone would be more extensive, but since power input is the same, evaporative cooling would likely dominate before the thermal wave runs its course. However, the larger critical radius should result in greater persistence of liquid for high initial ice concentration. We ran our numerical model for 40% and 50% ice content with a far-field and atmospheric temperature of 230K. As expected, the process of melting and drying was found to extend to slightly larger radii and to take considerably longer to run to completion. After approximately 500 sols, all the wet zones had been sterilized except for a small band at the deepest locations. Unlike the nominal case, a few such cells persisted even at 40% ice concentration. However, for both 40% and 50% ice, the cells in question were wet for less than 25 sols. Ice near 230K regolith would be extremely unstable and is not expected.

More plausible scenarios that might affect water persistence involve factors such as wind or salinity. Consider, for example, increasing the surface wind speed. In the thin atmosphere of Mars, water vapor is transported far more efficiently than on Earth (longer mean free path), while heat is transported far less efficiently (fewer molecules). The net effect of wind will thus be to remove water more efficiently from the surface (resulting in less-persistent water at depth), even though the surface may be slightly colder. A saline solution has a lower melting point and therefore a smaller sublimation rate at the melting point. Intuition might suggest that this would result in the formation of liquid farther from the heat source, water that would persist longer and be less prone to subsequent heat sterilization. However, the situation is considerably more complex than that because lowering the melting point modifies the thermal gradient on both the warm and the cold sides of the water layer, thus affecting the overall fraction of heat utilized for melting the ice.

Empirically, this has the effect of significantly *reducing* the persistence of water, as determined by running simulations with the melting point reduced by 5.58K, corresponding to a 3 Molar solution (saltier than typical seawater, less salty than the Dead Sea). In general, we do not expect the results of the briny scenario to be qualitatively different from those we have modeled, and the brine itself further constrains the types of microbes that might be capable of propagating.

Conclusions

We have examined scenarios for generation of liquid water on Mars by a local heat source such as a Radioactive Power Source. Since little is certain about the thermophysical properties of martian soil, we have selected parameters that are conservative but not pathological. The general approach was to develop simple steady-state models that allow the amount and persistence of liquid water to be determined rapidly over a wide range of parameters, then validating those models by performing detailed dynamical calculations for specific instances.

After a 250 W heat source is deposited in the icy regolith, a thermal wave propagates that melts and vaporizes ice in an expanding shell, eventually reaching quasi-equilibrium at a distance of tens of centimeters from the source. Temperatures in the desiccated inner region are sufficient for biological sterilization, but liquid can persist at the interface between the near-field desiccated region and the far-field icy region for a period of weeks to months. The single most important parameter is the initial ice content of the regolith, and water films are seen to persist only for the most ice-rich cases.

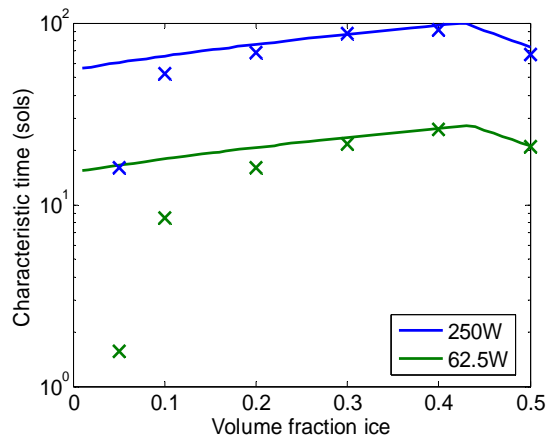


Figure 9. Comparison of the persistence of water between 1-D calculations (lines) and the numerical model (crosses). The calculations assume that i) 50% of the heat generated by the RPS is absorbed in a sphere bounded by the smaller of the critical radius or sublimation horizon, ii) 25% of that heat goes into warming or sublimating ice, and iii) the remainder of the absorbed heat goes into warming the dry soil. The numerical simulations are allowed to evolve without such restrictions.

Acknowledgements

<http://dx.doi.org/10.1029/2004JE002350>

This work was supported by NASA's 2009 Mars Science Laboratory project at the Jet Propulsion Laboratory, California Institute of Technology. The authors benefited greatly from discussions with Gaylon Campbell of the University of Washington.

References

- Abelson, R. D. (Ed.) et al. (2005) Expanding Frontiers with Standard Radioisotope Power Systems, NASA Document JPL D-28902
- Boynton, W. V. et al. (2002) "Distribution of hydrogen in the near surface of Mars: evidence for subsurface ice deposits" *Science* 297, 81-85.
<http://dx.doi.org/10.1126/science.1073722>
- Costard, F., F. Forget, N. Mangold and J. P. Peulvast (2002) "Formation of recent Martian debris flows by melting of near-surface ground ice at high obliquity" *Science* 295, 110-113.
<http://dx.doi.org/10.1126/science.1066698>
- Feldman, W. C. et al. (2002) "Global distribution of neutrons from Mars: results from Mars Odyssey" *Science* 297, 75-78. <http://dx.doi.org/10.1126/science.1073541>
- Gardner, W. R. (1968). "Availability and measurement of soil water" in *Water Deficits and Plant Growth*, Vol. 1, 107-135, Academic Press, New York.
- Hecht, M. H. (2002) "Metastability of liquid water on Mars" *Icarus* 156, 373-386.
<http://dx.doi.org/10.1006/icar.2001.6794>
- Hillel, D. (1998) *Environmental Soil Physics*, Academic Press, San Diego.
- Houben, H., R. M. Haberle, R. E. Young and A. P. Zent (1997) "Modeling the Martian seasonal water cycle" *Journal of Geophysical Research* 102, 9069-9084.
<http://dx.doi.org/10.1029/97JE00046>
- Ingersoll, A. P. (1970) "Mars: Occurrence of liquid water" *Science* 168, 972-973.
- Jakosky, B. M. (1985) "The seasonal cycle of water on Mars" *Space Science Reviews* 41, 131-200.
- Malin, M. C. and K. S. Edgett (2000) "Evidence for recent groundwater seepage and surface runoff on Mars" *Science* 288, 2330-2335.
- Mellon, M. T., B. M. Jakosky and S. E. Postawko (1997) "The persistence of equatorial ground ice on Mars" *Journal of Geophysical Research* 102, 19357-19370.
<http://dx.doi.org/10.1029/97JE01346>
- Mellon, M. T., W. C. Feldman and T. H. Prettyman (2004) "The presence and stability of ground ice in the southern hemisphere of Mars" *Icarus* 169, 324-340.
<http://dx.doi.org/10.1016/j.icarus.2003.10.022>
- Mitrofanov, I. et al. (2002) "Maps of subsurface hydrogen from the high energy neutron detector, Mars Odyssey" *Science* 197, 78-81.
<http://dx.doi.org/10.1126/science.1073616>
- Putzig, N. E., M. T. Mellon, K. A. Kretke and R. E. Arvidson (2005) "Global thermal inertia and surface properties of Mars from the MGS mapping mission" *Icarus* 173, 325-341.
<http://dx.doi.org/10.1016/j.icarus.2004.08.017>
- Richardson, M. I. and R. J. Wilson (2002) "Investigation of the nature and stability of the Martian seasonal water cycle with a general circulation model" *Journal of Geophysical Research* 107(E5), 5031.
<http://dx.doi.org/10.1029/2001JE001536>
- Schorghofer, N. and O. Aharonson (2005) "Stability and exchange of subsurface ice on Mars" *Journal of Geophysical Research* 110, E05003.